Geometry of river networks. II. Distributions of component size and number

Peter Sheridan Dodds[1,2,*] and Daniel H. Rothman[2,†]
[1]*Department of Mathematics, Massachusetts Institute of Technology, Cambridge, Massachusetts 02139*
[2]*Department of Earth, Atmospheric and Planetary Sciences, Massachusetts Institute of Technology, Cambridge, Massachusetts 02139*
(Received 18 May 2000; published 27 December 2000)

The structure of a river network may be seen as a discrete set of nested subnetworks built out of individual stream segments. These network components are assigned an integral stream order via a hierarchical and discrete ordering method. Exponential relationships, known as Horton's laws, between stream order and ensemble-averaged quantities pertaining to network components are observed. We extend these observations to incorporate fluctuations and all higher moments by developing functional relationships between distributions. The relationships determined are drawn from a combination of theoretical analysis, analysis of real river networks including the Mississippi, Amazon, and Nile, and numerical simulations on a model of directed, random networks. Underlying distributions of stream segment lengths are identified as exponential. Combinations of these distributions form single-humped distributions with exponential tails, the sums of which are in turn shown to give power-law distributions of stream lengths. Distributions of basin area and stream segment frequency are also addressed. The calculations identify a single length scale as a measure of size fluctuations in network components. This article is the second in a series of three addressing the geometry of river networks.

DOI: 10.1103/PhysRevE.63.016116 PACS number(s): 64.60.Ht, 92.40.Fb, 92.40.Gc, 68.70.+w

I. INTRODUCTION

Branching networks are an important category of all networks with river networks being a paradigmatic example. Probably as much as any other natural phenomena, river networks are a rich source of scaling laws [1–3]. Central quantities such as drainage basin area and stream lengths are reported to closely obey power-law statistics [1–8]. The origin of this scaling has been attributed to a variety of mechanisms including, among others, principles of optimality [1,9], self-organized criticality [10], invasion percolation [11], and random fluctuations [3,12–14]. One of the difficulties in establishing any theory is that the reported values of scaling exponents show some variation [6,7,15].

With this variation in mind, we have [16] extensively examined Hack's law, the scaling relationship between basin shape and stream length. Such scaling laws are inherently broad brushed in their descriptive content. In an effort to further improve comparisons between theory and data and, more importantly, between networks themselves, we consider here a generalization of Horton's laws [17,18]. Defined fully in the following section, Horton's laws describe how average values of network parameters change with a certain discrete renormalization of the network. The introduction of these laws by Horton may be seen as one of many examples that presaged the theory of fractal geometry [19]. In essence, they express the relative frequency and size of network components such as stream segments and drainage basins.

Here, we extend Horton's laws to functional relationships between probability distributions, rather than simply average values. The recent work of Peckham and Gupta was the first to address this natural generalization of Horton's laws [20]. Our work agrees with their findings, but goes further to characterize the distributions and develop theoretical links between the distributions of several different parameters. We also present empirical studies that reveal underlying scaling functions with a focus on fluctuations and further consider deviations due to finite-size effects.

We examine continent-scale networks: the Mississippi, Amazon, Congo, Nile, and Kansas river basins. As in [16], we also examine Scheidegger's model of directed, random networks [13]. Both real and model networks provide important tests and motivations for our generalizations of Horton's laws.

We begin with definitions of stream ordering and Horton's laws. Thereafter, the paper is divided into two main sections. In Sec. III, we first sketch the theoretical generalization of Horton's laws. Estimates of the Horton ratios are carried out in Sec. IV and these provide basic parameters of the generalized laws. Empirical evidence from real continent-scale networks is then provided along with data from Scheidegger's random network model in Sec. V. In Sec. VI, we derive the higher-order moments for stream length distributions, and in Sec. VII, we consider deviations from Horton's laws for large basins. In the Appendix, we expand on some of the connections outlined in Sec. V, presenting a number of mathematical considerations on these generalized Horton distributions.

This paper is the second in a series of three on the geometry of river networks. In the first [16], we addressed issues of scaling and universality and provided further motivation for our general investigation. In the third article of the series [21], we extend the work of the present paper by examining the detailed architecture of river networks, i.e., how network components fit together.

*Author to whom correspondence should be addressed. Electronic address: dodds@segovia.mit.edu; URL: http://segovia.mit.edu/
†Electronic address: dan@segovia.mit.edu

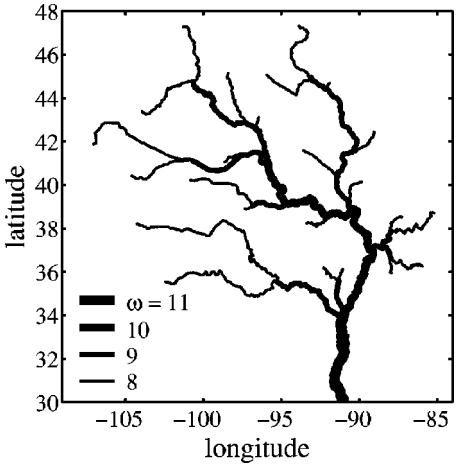

FIG. 1. Stream segments for $\omega=8$ up to $\omega=\Omega=11$ for the Mississippi River. The spherical coordinates of latitude and longitude (measured here in degrees) are used and the scale corresponds to roughly 2000 km along each axis.

II. STREAM ORDERING AND HORTON'S LAWS

Stream ordering was first introduced by Horton in an effort to quantify the features of river networks [17]. The method was later improved by Strahler to give the present technique of Horton-Strahler stream ordering [22]. Stream ordering is a method applicable to any field where branching, hierarchical networks are important. Indeed, much use of stream ordering has been made outside of the context of river networks, a good example being the study of venous and arterial blood networks in biology [23–30]. We describe two conceptions of the method and then discuss empirical laws defined within the context of stream ordering.

A network's constituent stream segments are ordered by an iterative pruning. An example of stream ordering for the Mississippi basin is shown in Fig. 1. A source stream is defined as a section of stream that runs from a channel head to a junction with another stream (for an arboreal analogy, think of the leaves of a tree). These source streams are classified as the first-order stream segments of the network. Next, remove these source streams and identify the new source streams of the remaining network. These are the second-order stream segments. The process is repeated until one stream segment is left of order Ω. The order of the network is then defined to be Ω.

Once stream ordering on a network has been done, a number of natural quantities arise. These include n_ω, the number of basins (or equivalently stream segments) for a given order ω; $\overline{l}_\omega$, the average main stream length; $\overline{l^{(s)}_\omega}$, the average stream segment length; $\overline{a}_\omega$, the average basin area; and the variation in these numbers from order to order. Horton [17] and later Schumm [18] observed that the following ratios are generally independent of order ω:

$$\frac{n_\omega}{n_{\omega+1}}=R_n, \quad \frac{\overline{l}_{\omega+1}}{\overline{l}_\omega}=R_l, \quad \frac{\overline{a}_{\omega+1}}{\overline{a}_\omega}=R_a. \tag{1}$$

Since the main stream length averages $\overline{l}_\omega$ are combinations of stream segment lengths $\overline{l}_\omega=\Sigma_{\nu=1}^{\omega}\overline{l^{(s)}_\omega}$, we have that the Horton ratio for stream segment lengths $R_{l(s)}$ is equivalent to R_l. Because our theory will start with distributions of the $l^{(s)}_\omega$, we will generally use the ratio $R_{l(s)}$ in place of R_l.

Horton's laws have remained something of a mystery in geomorphology—the study of earth surface processes and form—due to their apparent robustness and hence perceived lack of physical (or geological) content. However, statements that Horton's laws are ''statistically inevitable'' [31], while possibly true, have not yet been based on reasonable assumptions [3]. Furthermore, many other scaling laws can be shown to follow in part from Horton's laws [8]. Thus, Horton's laws being without content would imply the same is true for those scaling laws that follow from them. Other sufficient assumptions include uniform drainage density (i.e., networks are space-filling) and self-affinity of single channels. The latter can be expressed as the relation [7,32–34]

$$l\propto L_\parallel^d, \tag{2}$$

where $L_\parallel$ is the longitudinal diameter of a basin. Scaling relations may be derived and the set of relevant scaling exponents can be reduced to just two: d as given above and the ratio $\ln R_{l(s)}/\ln R_n$ [8]. Note that one obtains $R_a\equiv R_n$ so that only the two Horton ratios R_n and $R_{l(s)}$ are independent. Horton ratios are thus of central importance in the full theory of scaling for river networks.

III. POSTULATED FORM OF HORTON DISTRIBUTIONS

Horton's laws relate quantities that are indexed by a discrete set of numbers, namely the stream orders. They also algebraically relate mean quantities such as $\overline{a}_\omega$. Hence, we may consider a generalization to functional relationships between probability distributions. In other words, for stream lengths and drainage areas, we can explore the relationships between probability distributions defined for each order.

Furthermore, as we have noted, Horton's laws can be used to derive power laws of continuous variables such as the probability distributions of drainage area a and main stream length l [7,8,35]:

$$P(a)\propto a^{-\tau}, \quad P(l)\propto l^{-\gamma}. \tag{3}$$

These derivations necessarily only give discrete points of power laws. In other words, the derivations give points as functions of the discrete stream order ω and are uniformly spaced logarithmically and we interpolate the power law from there. The distributions for stream lengths and areas must therefore have structures that when combined across orders produce smooth power laws.

For the example of the stream segment length $l^{(s)}_\omega$, Horton's laws state that the mean $\overline{l^{(s)}_\omega}$ grows by a factor of $R_{l(s)}$ with each integer step in order ω. In considering $P(l^{(s)}_\omega,\omega)$, the underlying probability distribution function for $l^{(s)}_\omega$, we postulate that Horton's laws apply for every moment of the distribution and not just the mean. This generalization of Horton's laws may be encapsulated in a statement about the distribution $P(l^{(s)}_\omega,\omega)$ as

$$P(l_\omega^{(s)},\omega)=C_{l^{(s)}}(R_nR_{l^{(s)}})^{-\omega}F_{l^{(s)}}(l_\omega^{(s)}R_{l^{(s)}}^{-\omega}). \quad (4)$$

The factor of $(R_n)^{-\omega}$ indicates that $\int_{l^{(s)}=0}^{\infty}dl^{(s)}P(l_\omega^{(s)},\omega) \propto (R_n)^{-\omega}$, i.e., the frequency of stream segments of order ω decays according to Horton's law of stream number given in Eq. (1). Similarly, for l_ω, a_ω, and $n_{\Omega,\omega}$, we write

$$P(l_\omega,\omega)=C_l(R_nR_{l^{(s)}})^{-\omega}F_l(l_\omega R_{l^{(s)}}^{-\omega}), \quad (5)$$

$$P(a_\omega,\omega)=C_a(R_n^2)^{-\omega}F_a(a_\omega R_n^{-\omega}), \quad (6)$$

and

$$P(n_{\Omega,\omega})=C_n(R_n)^{\Omega-\omega}F_n(n_{\Omega,\omega}R_n^{-\omega}), \quad (7)$$

where constants $C_{l^{(s)}}$, C_l, C_a, and c_n are appropriate normalizations. We have used the subscripted versions of the lengths and areas, $l_\omega^{(s)}$, l_ω, and a_ω, to reinforce that these parameters are for points at the outlets of order ω basins only. The quantity $n_{\Omega,\omega}$ is the number of streams of order ω within a basin of order Ω. This will help with some notational issues later on. The form of the distribution functions $F_{l^{(s)}}$, F_l, F_a, and F_n and their interrelationships become the focus of our investigations. Since scaling is inherent in each of these postulated generalizations of Horton's laws, we will often refer to these distribution functions as *scaling functions*.

We further postulate that distributions of stream segment lengths are best approximated by exponential distributions. Empirical evidence for this will be provided later on in Sec. V. The normalized scaling function $F_{l^{(s)}}(u)$ of Eq. (4) then has the form

$$F_{l^{(s)}}(u)=\frac{1}{\xi}e^{-u/\xi}=F_{l^{(s)}}(u;\xi), \quad (8)$$

where we have introduced a new length scale ξ and stated its appearance with the notation $F_{l^{(s)}}(u;\xi)$. The value of ξ is potentially network dependent. As we will show, distributions of main stream lengths, areas, and stream number are all dependent on ξ and this is the only additional parameter necessary for their description. Note that ξ is both the mean and standard deviation of $F_{l^{(s)}}(u;\xi)$, i.e., for exponential distributions, fluctuations of a variable are on the order of its mean value. We may therefore think of ξ as a *fluctuation length scale*. Note that the presence of exponential distributions indicates a randomness in the physical distribution of streams themselves and this is largely the topic of our third paper [21].

Since main stream lengths are combinations of stream segment lengths, i.e., $l_\omega=\Sigma_{i=1}^{\omega}l_\omega^{(s)}$, we have that the distributions of main stream lengths of order ω basins are approximated by convolutions of the stream segment length distributions. For this step, it is more appropriate to use conditional probabilities such as $P(l_\omega^{(s)}|\omega)$ where the basin order ω is taken to be fixed. We thus write

$$P(l_\omega|\omega)=P(l_1^{(s)}|1)*P(l_2^{(s)}|2)*\cdots*P(l_\omega^{(s)}|\omega), \quad (9)$$

where $*$ denotes convolution. Details of the form obtained are given in section 1 of the Appendix.

The next step takes us to the power-law distribution for main stream lengths. Summing over all stream orders and integrating over $u=l_\omega$ we have

$$P(l)\simeq\sum_{\omega=1}^{\infty}\int_{u=l}^{\infty}du\,P(u,\omega), \quad (10)$$

where we have returned to the joint probability for this calculation. The integral over u is replaced by a sum when networks are considered on discrete lattices. Note that the probability of finding a main stream of length l is independent of any sort of stream ordering since it is defined on an unordered network. The details of this calculation may be found in section 2 of the Appendix, where it is shown that a power law $P(l)\propto l^{-\gamma}$ follows from the deduced form of the $P(l_\omega,\omega)$ with $\gamma=\ln R_n/\ln R_{l^{(s)}}$.

IV. ESTIMATION OF HORTON RATIOS

We now examine the usual Horton laws in order to estimate the Horton ratios. These ratios are seen as intrinsic parameters in the probability distribution functions given above in Eqs. (4)–(7).

Figure 2(a) shows the stream order averages of $l^{(s)}$, l, a, and n for the Mississippi basin. Deviations from exponential trends of Horton's laws are evident and indicated by deviations from straight lines on the semilogarithmic axis. Such deviations are to be expected for the smallest and largest orders within a basin [8,21]. For the smallest orders, the scale of the grid used becomes an issue but even with infinite resolution, the scaling of lengths, areas, and number for low orders cannot all hold at the same time [8]. For large orders, the decrease in sample space contributes to these fluctuations since the number of samples of order ω streams decays exponentially with order as $(R_n)^{\Omega-\omega}$. Furthermore, correlations with overall basin shape provide another source of deviations [21]. Nevertheless, in our theoretical investigations below, we will presume exact scaling. Note also that the equivalence of R_n and R_a is supported by Fig. 2(b) where the stream numbers n_w have been inverted for comparison. Similar agreement is found for the Amazon and Nile as shown in Tables I, II, and III, which we now discuss.

Table I shows the results of regression on the Mississippi data for various ranges of stream orders for stream number, area, and lengths. Tables II and III show the same results carried out for the Amazon and Nile. Each table presents estimates of the four ratios R_n, R_a, R_l, and $R_{l^{(s)}}$. Also included are the comparisons R_a/R_n and $R_l/R_{l^{(s)}}$, both of which we expect to be close to unity. For each quantity, we calculate the mean μ, standard deviation σ, and normalized deviation σ/μ.

Note the variation of exponents with choice of order range. This is the largest source of error in the calculation of the Horton ratios. Therefore, rather than taking a single range of stream orders for the regression, we examine a collection of ranges. Also, the deviations for high and low orders observed in Figs. 2(a) and 2(b) do of course affect measure-

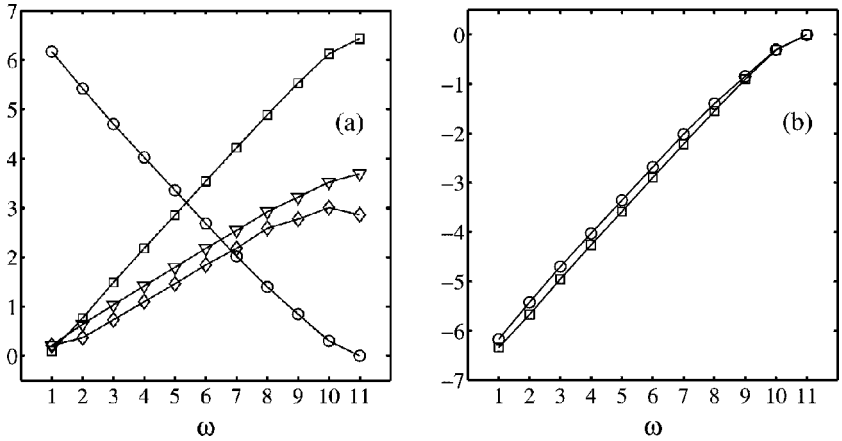

FIG. 2. Horton's laws for the order $\Omega = 11$ Mississippi river basin network. For (a), the ordinate axis is logarithmic (base 10) representing the number for stream number n_ω (circles), km^2 for area $\overline{a}_\omega$ (squares), and km for both main stream length $\overline{l}_\omega$ (triangles) and stream segment length $\overline{l}_\omega^{(s)}$ (diamonds). The stream order ω is dimensionless. Note the good agreement between $\overline{l}_\omega$ and $\overline{l}_\omega^{(s)}$. In (b), the stream number data n_ω (circles) has been inverted from that in (a), i.e., the plot is of n_ω^{-1}. This is compared with the dimensionless $\overline{a}_\omega/\overline{a}_\Omega$ (squares) showing good support for the prediction that the slopes are equal, i.e., $R_a \equiv R_n$.

ments of the Horton ratios. In all cases, we have avoided using data for the smallest and largest orders.

For the three example networks given here, the statements $R_a \equiv R_n$ and $R_l \equiv R_{l^{(s)}}$ are well supported. The majority of ranges give R_n/R_a and $R_l/R_{l^{(s)}}$ very close to unity. The averages are also close to 1 and are different from unity mostly by within 1.0 and uniformly by within 1.5 standard deviations.

The normalized deviations, i.e., σ/μ, for the four ratios are all below 0.05. No systematic ordering of the σ/μ is observed. Of all the data, the values for R_l in the case of the Mississippi are the most notably uniform having $\sigma/\mu = 0.015$. Throughout there is a slight trend for regression on lower orders to overestimate and on higher orders to underestimate the average ratios, while reasonable consistency is found at intermediate orders.

Thus, overall the ranges chosen in the tables give a reasonably even set of estimates of the Horton ratios and we will use these averages as our estimates of the ratios.

V. EMPIRICAL EVIDENCE FOR HORTON DISTRIBUTIONS

A. Stream segment length distributions

We now present Horton distributions for the Mississippi, Amazon, and Nile river basins as well as the Scheidegger

TABLE I. Horton ratios for the Mississippi River [36]. For each range of orders (ω_1, ω_2), estimates of the ratios are obtained via simple regression analysis. For each quantity, a mean μ, standard deviation σ and normalized deviation σ/μ are calculated. All ranges with $2 \leqslant \omega_1 < \omega_2 \leqslant 8$ are used in these estimates, but not all are shown. The values obtained for R_l are especially robust while some variation is observed for the estimates of R_n and R_a. Good agreement is observed between the ratios R_n and R_a and also between R_l and $R_{l^{(s)}}$.

ω range	R_n	R_a	R_l	$R_{l^{(s)}}$	R_a/R_n	$R_l/R_{l^{(s)}}$
[2,3]	5.27	5.26	2.48	2.30	1.00	1.07
[2,5]	4.86	4.96	2.42	2.31	1.02	1.05
[2,7]	4.77	4.88	2.40	2.31	1.02	1.04
[3,4]	4.72	4.91	2.41	2.34	1.04	1.03
[3,6]	4.70	4.83	2.40	2.35	1.03	1.03
[3,8]	4.60	4.79	2.38	2.34	1.04	1.02
[4,6]	4.69	4.81	2.40	2.36	1.02	1.02
[4,8]	4.57	4.77	2.38	2.34	1.05	1.01
[5,7]	4.68	4.83	2.36	2.29	1.03	1.03
[6,7]	4.63	4.76	2.30	2.16	1.03	1.07
[7,8]	4.16	4.67	2.41	2.56	1.12	0.94
Mean μ	4.69	4.85	2.40	2.33	1.04	1.03
Standard deviation σ	0.21	0.13	0.04	0.07	0.03	0.03
σ/μ	0.045	0.027	0.015	0.031	0.024	0.027

TABLE II. Horton ratios for the Amazon [37]. Details are as per Table I.

ω range	R_n	R_a	R_l	$R_{l(s)}$	R_a/R_n	$R_l/R_{l(s)}$
[2,3]	5.05	4.69	2.10	1.65	0.93	1.28
[2,5]	4.65	4.64	2.11	1.92	1.00	1.10
[2,7]	4.54	4.63	2.16	2.11	1.02	1.03
[3,4]	4.54	4.73	2.10	2.01	1.04	1.05
[3,6]	4.51	4.62	2.15	2.15	1.02	1.00
[3,8]	4.44	4.55	2.19	2.23	1.02	0.98
[4,6]	4.52	4.59	2.18	2.24	1.02	0.97
[4,8]	4.42	4.51	2.21	2.27	1.02	0.97
[5,7]	4.39	4.62	2.25	2.39	1.05	0.94
[6,7]	4.19	4.55	2.26	2.40	1.09	0.94
[7,8]	4.50	4.21	2.15	2.12	0.94	1.02
Mean μ	4.51	4.58	2.17	2.15	1.01	1.02
Standard deviation σ	0.17	0.12	0.05	0.19	0.03	0.08
σ/μ	0.038	0.026	0.024	0.089	0.034	0.078

model. Scheidegger networks may be thought of as collections of random-walker streams and are fully defined in [16] and extensively studied in [21]. The forms of all distributions are observed to be the same in the real data and in the model.

The first distribution is shown in Fig. 3(a). This is the probability density function of $l_4^{(s)}$ fourth-order stream segment lengths, for the Mississippi River. Distributions for different orders can be rescaled to show satisfactory agreement. This is done using the postulated Horton distribution of stream segment lengths given in Eq. (4). The rescaling is shown in Fig. 3(b) and is for orders $\omega=3,\ldots,6$. Note that the effect of the exponential decrease in the number of samples with order is evident for $\omega=6$ since $P(l_6^{(s)})$ is considerably scattered. Nevertheless, the figure shows the form of these distributions to be most closely approximated by exponentials. We observe similar exponential distributions for the Amazon, the Nile, and the Scheidegger model. The fluctuation length scale ξ is found to be approximately 800 m for the Mississippi, 1600 m for the Amazon, and 1200 m for the Nile.

Since ξ is based on the definition of stream ordering, comparisons of ξ are only sensible for networks that are measured on topographies with the same resolution. The above values of ξ are approximate and our confidence in them would be improved with higher-resolution data. Nevertheless, they do suggest that fluctuations in network structure increase as we move from the Mississippi through to the Nile, and then the Amazon.

B. Main stream segment length distributions

The distributions of $\omega=4$ main stream lengths for the Amazon River are shown in Fig. 4(a). Since main stream lengths are sums of stream segment lengths, their distribution has a single peak away from the origin. However, these distributions will not tend towards a Gaussian because the individual stream length distributions do not satisfy the requirements of the central limit theorem [39]. This is because the moments of the stream segment length distributions grow exponentially with stream order. As the semilogarithmic axes indicate, the tail may be reasonably well (but not exactly) modeled by exponentials. There is some variation in the distribution tails from region to region. For example, corresponding distributions for the Mississippi data do exhibit tails that are closer to exponentials. However, for the

TABLE III. Horton ratios for the Nile [38]. Details are as per Table I. Here $2\leqslant\omega_1<\omega_2\leqslant 7$.

ω range	R_n	R_a	R_l	$R_{l(s)}$	R_a/R_n	$R_l/R_{l(s)}$
[2,3]	4.78	4.71	2.47	2.08	0.99	1.19
[2,5]	4.55	4.58	2.32	2.12	1.01	1.10
[2,7]	4.42	4.53	2.24	2.10	1.02	1.07
[3,5]	4.45	4.52	2.26	2.14	1.01	1.06
[3,7]	4.35	4.49	2.20	2.10	1.03	1.05
[4,6]	4.38	4.54	2.22	2.18	1.03	1.02
[5,6]	4.38	4.62	2.22	2.21	1.06	1.00
[6,7]	4.08	4.27	2.05	1.83	1.05	1.12
Mean μ	4.42	4.53	2.25	2.10	1.02	1.07
Standard deviation σ	0.17	0.10	0.10	0.09	0.02	0.05
σ/μ	0.038	0.023	0.045	0.042	0.019	0.045

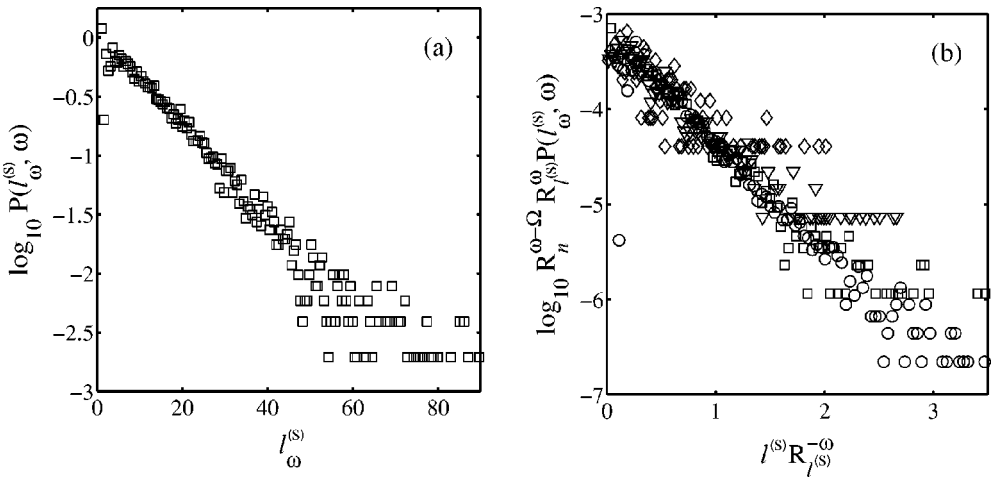

FIG. 3. Plot (a) shows an example distribution of stream segment lengths, $P(l_\omega^{(s)},\omega)$, for the Mississippi for order $\omega=4$. The lengths here are in kilometers. The semilogarithmic axes indicate the distribution is well approximated by an exponential. The value of the length scale ξ [see Eq. (8)] is estimated to be approximately 800 m. Rescaled versions of the same stream segment length distributions for $\omega=3$ (circles), $\omega=4$ (squares), $\omega=5$ (triangles), and $\omega=6$ (diamonds), are shown in (b). The rescaling is done according to Eq. (4). The values of the Horton ratios used are $R_n=4.69$ and $R_{l^{(s)}}=2.33$ as determined from Table I.

present work where we are attempting to characterize the basic forms of the Horton distributions, we consider these deviations to be of a higher-order nature and belonging to the realm of further research.

In accord with Eq. (5), Fig. 4(b) shows the rescaling of the main stream length distributions for $\omega=3,\ldots,6$. The ratios used, $R_n=4.49$ and $R_l=2.19(\simeq R_{l^{(s)}}=2.17)$ are taken from Table II. Given the scatter of the distributions, it is unreasonable to perform minimization techniques on the rescaled data itself in order to estimate R_n and R_l. This is best done by examining means, as we have done, and higher-order moments, which we discuss below. Furthermore, varying R_n and R_l from the above values by, say, ± 0.05 does not greatly distort the visual quality of the ''data collapse.''

Similar results for the Scheidegger model are shown in Fig. 5. The Scheidegger model may be thought of as a network defined on a triangular lattice where at each lattice site one of two directions is chosen as the stream path [16,21]. Figure 5(a) gives a single example distribution for main stream lengths of order $\omega=6$ basins. The tail is exponential as per the real world data. Figure 5(b) shows a collapse of main stream length distributions for orders $\omega=4$ through 7. In contrast to the real data where an overall basin order is fixed (Ω), there is no maximum basin order here. The distributions in Fig. 5(b) have an arbitrary normalization, meaning that the absolute values of the ordinate are also arbitrary. Otherwise, this is the same collapse as given in Eq. (5). For the Scheidegger model, our simulations yield $R_n\simeq 5.20$ and $R_{l^{(s)}}\simeq 3.00$ [8]. For all distributions, we observe similar functional forms for real networks and the Scheidegger model, the only difference lying in parameters such as the Horton ratios.

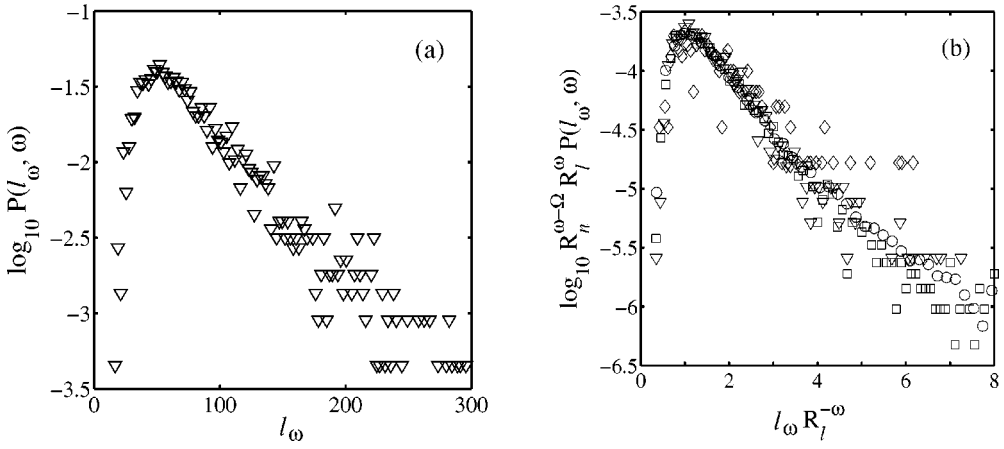

FIG. 4. Plot (a) shows an example distribution for order $\omega=5$ main stream lengths (measured in kilometers) for the Amazon. The distribution is unimodal with what is a reasonable approximation of an exponential tail. In (b), distributions of main stream length for $\omega=3$ (circles), $\omega=4$ (squares), $\omega=5$ (triangles), and $\omega=6$ (diamonds) are rescaled according to Eq. (5). The values of the Horton ratios used here are $R_n=4.51$ and $R_{l^{(s)}}=2.17$, taken from Table II.

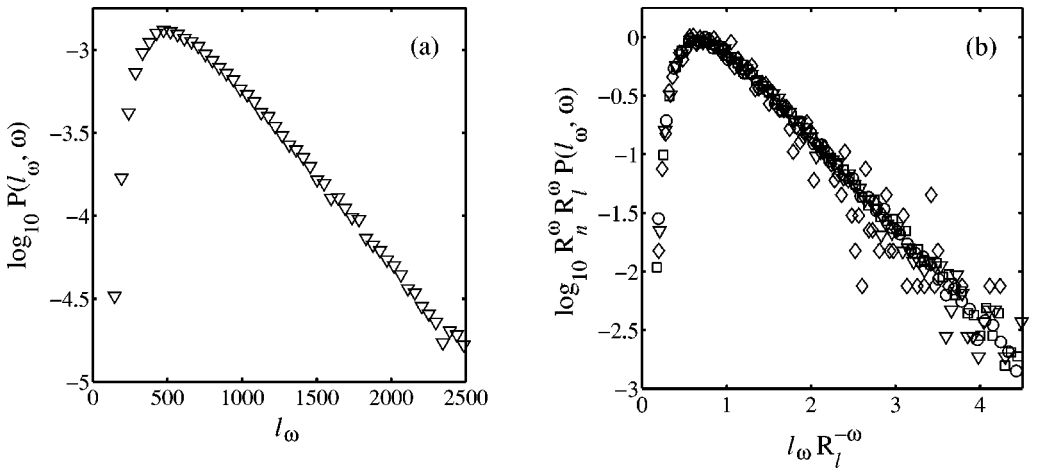

FIG. 5. Given in (a) is an example distribution of order $\omega=6$ main stream lengths for the Scheidegger model. Lengths are given in arbitrary lattice units. The same form is observed as for real networks such as the Amazon (Fig. 4). In the same way as Fig. 4(b), (b) show rescaled distributions of main stream length for $\omega=4$ (circles), $\omega=5$ (squares), $\omega=6$ (triangles), and $\omega=7$ (diamonds). Note that in (b), distributions are not normalized with respect to a fixed basin order Ω and hence the vertical offset is arbitrary. The values of the ratios used here are $R_n \simeq 5.20$ and $R_l \simeq 3.00$ [8].

C. Drainage area distributions

Figure 6 shows more Horton distributions, this time for drainage area as calculated for the Nile river basin. In Fig. 6, an example distribution for $\omega=4$ subbasins is presented. The distribution is similar in form to those of main stream lengths of Fig. 4, again showing a reasonably clear exponential tail. Rescaled drainage area distributions for $\omega=3,\ldots,6$ are presented in Fig. 6(b). The rescaling now follows Eq. (6). Note that if R_n and R_a were not equivalent, the rescaling would be of the form

$$P(a_\omega,\omega)=C_a(R_nR_a)s^{-\omega}F_a(a_\omega R_a^{-\omega}). \tag{11}$$

Since we have asserted that $R_n \equiv R_a$, Eq. (11) reduces to Eq. (6). The Horton ratio used here is $R_n=4.42$, which is in good agreement with $R_a=4.53$, the respective standard deviations being 0.17 and 0.10. Both figures are taken from the data of Table III.

D. Summing distributions to form power laws

As stated in Sec. III, the Horton distributions of a_ω and l_ω must combine to form power-law distributions for a and l [see Eqs. (3) and (10)]. Figure 7 provides empirical support for this observation for the example main stream lengths of the Mississippi network. The distributions for $\omega=3$, 4, and 5 main stream lengths are individually shown. Their combination together with the distribution of l_6 gives the reasonable approximation of a power law as shown. The area distributions combine in the same way. Note that the distributions do not greatly overlap. Each point of the power law is therefore

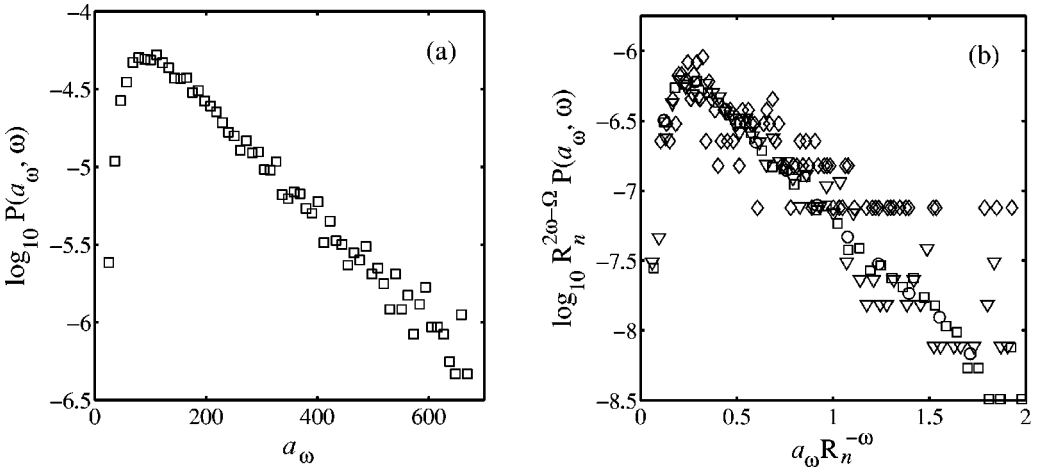

FIG. 6. The distribution of drainage areas for $\omega=4$ subbasins of the Nile are shown in (a). All areas are measured in km^2. An exponential tail is observed as per the distributions of stream segment length (Fig. 3) and main stream length (Fig. 4). In (b), distributions of drainage area for $\omega=3$ (circles), $\omega=4$ (squares), $\omega=5$ (triangles), and $\omega=6$ (diamonds), are rescaled according to Eq. (6). The rescaling uses the estimate $R_n=4.42$ found in Table III.

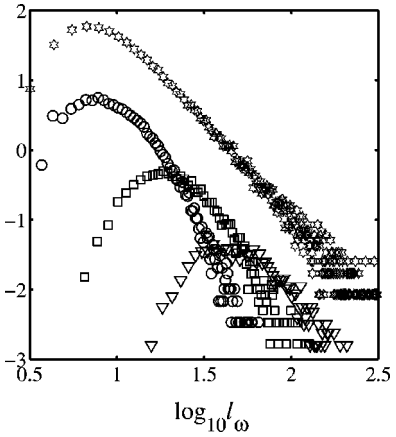

FIG. 7. Summation of main stream length distributions for the Mississippi. Both axes are logarithmic, the unit of length is the kilometer and the vertical axis is probability density with units of km^{-1}. Distributions of l_ω for orders $\omega=3$ (circles), $\omega=4$ (squares), and $\omega=5$ (triangles), are shown. As expected, the distributions sum together to give a power-law tail (stars). The power-law distribution (which is vertically offset by an order of magnitude for clarity) is the summation of the distributions below as well as the distribution for order $\omega=6$ main stream lengths.

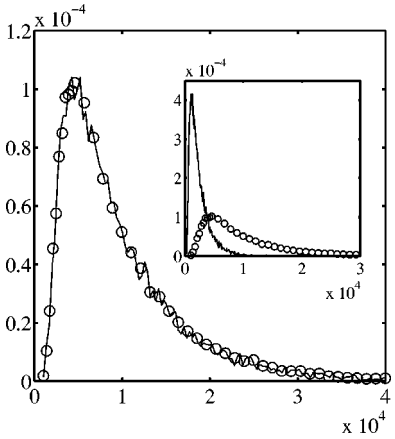

FIG. 8. Comparison of number and area distributions for the Scheidegger model. Area is in terms of square lattice units. In the inset plot, the raw distributions shown are $P(a_6|6)$ (circles) and $P(n_{6,1}|6)$ (continuous line). The latter is the probability of finding $n_{6,1}$ source streams in an order $\omega=6$ basin. In the main plot, the number distribution has been rescaled to be $1/4P(n_{6,1}|6)$ as a function of $4n_{6,1}$ and the area distribution is unrescaled (the symbols are the same as for the inset plot). For the Scheidegger model, source streams occur at any site with probability of 1/4, hence the rescaling by a factor of 4.

the addition of significant contributions from only two or three of the separate distributions. The challenge here then is to understand how rescaled versions of F_l, being the basic form of the $P(l_\omega,\omega)$, fit together in such a clean fashion. The details of this connection are established in section 2 of the Appendix.

E. Connecting distributions of number and area

In considering the generalized Horton distributions for number and area, we observe two main points: a calculation in the vein of what we are able to do for main stream lengths is difficult; and, the Horton distributions for area and number are equivalent.

In principle, Horton area distributions may be derived from stream segment length distributions. This follows from an assumption of statistically uniform drainage density, which means that the typical drainage area drained per unit length of any stream is invariant in space. Apart from the possibility of changing with space, which we will preclude by assumption, drainage density does naturally fluctuate as well [16]. Thus, we can write $a \simeq \rho \Sigma_\omega l_\omega^{(s)}$, where the sum is over all orders and all stream segments and ρ is the average drainage density.

However, we need to know, for an example basin, how many instances of each stream segment occur as a function of order. For example, the number of first-order streams in an order Ω basin is $n_{\Omega,1}$. Given the distribution of this number, we can then calculate the distribution of the total contribution of drainage area due to first-order streams. But the distributions of $n_{\Omega,\omega}$ are not independent, so we cannot proceed in this direction.

We could potentially use the typical number of order ω streams, $(R_n)^{\Omega-\omega}$. Then, the distribution of total area drained due to order ω streams would approach Gaussian because the individual distributions are identical and the central limit theorem would apply. However, because the fluctuations in the total number of stream segments are so great, we lose too much information with this approach. Indeed, the distribution of area drained by order ω stream segments in a basin reflects variations in their number rather than length. Again, we meet up with the problem of the numbers of distinct orders of stream segment lengths being dependent.

One final way would be to use Tokunaga's law [8,40–43]. Tokunaga's law states that the number of order ν side branches along an (absorbing) stream segment of order μ is given by

$$T_k = T_1 (R_{l^{(s)}})^{k-1}, \tag{12}$$

where $k=\mu-\nu$. The parameter T_1 is the average number of side streams having order $\nu=\mu-1$ for every order μ absorbing stream. This gives a picture of how a network fits together and may be seen to be equivalent to Horton's laws [8]. Now, even though we also understand the distributions underlying Tokunaga's law [16], similar technical problems arise. On descending into a network, we find the number of stream segments at each level to be dependent on all of the above.

Nevertheless, we can understand the relationship between the distributions for area and number. What follows is a generalization of the finding that $R_n \equiv R_a$. The postulated forms for these distributions were given in Eqs. (6) and (7). Consider $n_{\Omega,1}$, the number of first-order streams in an order Ω basin. Assuming that, on average, first-order streams are distributed evenly throughout a network, then this number is simply proportional to a_Ω. As an example, Fig. 8 shows data obtained for the Scheidegger model. For the Scheidegger model, first-order streams are initiated with a 1/4 probability

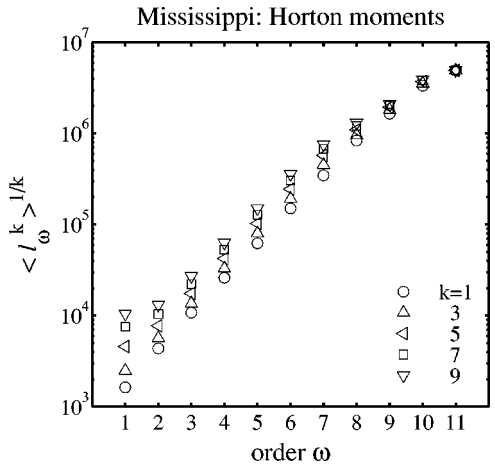

FIG. 9. A comparison of moments calculated for main stream length distributions for the Mississippi River. Lengths are in kilometers.

when the flow at the two upstream sites is randomly directed away, each with probability 1/2. Thus, for an area a_Ω, we expect and find $n_{\Omega,\omega}=a_\Omega/4$.

For higher internal orders, we can apply a simple renormalization. Assuming a system with exact scaling, the number of streams $n_{\Omega,\omega}$ is statistically equivalent to $n_{\Omega-\omega+1,1}$. Since the latter is proportional to $a_{\Omega-\omega+1}$, we have that

$$n_{\omega,\omega} \simeq \rho_\omega a_{\Omega-\omega+1}, \tag{13}$$

where the constant of proportionality is the density of order ω streams, Clearly, this equivalence improves as number increases, i.e., the difference $\Omega-\omega$ increases.

While we do not have exact forms for the area or number distributions, we note that they are similar to the main stream length distributions. Since source streams are linear basins with the width of a grid cell, the distribution of a_1 is the same as the distribution of l_1 and $l_1^{(s)}$, a pure exponential. Hence, $n_{\Omega,\Omega-1}$ is also an exponential. For increasing ω, the distribution of a_ω becomes single peaked with an exponential tail, qualitatively the same as the main stream length distributions.

VI. HIGHER-ORDER MOMENTS

Finally, we discuss the higher-order moments for the generalized Horton distributions. Figure 9 presents moments for distributions of main stream lengths for the case of the Mississippi. These moments are calculated directly from the main stream length distributions. A regular logarithmic spacing is apparent in moments for orders ranging from 3 to 7.

To see whether or not this is expected, we detail a few small calculations concerning moments starting from the exponential form of stream segment lengths given in Eq. (8). As noted previously, for an exponential distribution, $F_{l^{(s)}}(u)=\xi^{-1}e^{-u/\xi}$, the mean is simply $\langle u\rangle=\xi$. In general, the qth moment of an exponential distribution is

$$\langle u^q\rangle = \int_{u=0}^{\infty} \frac{u^q}{\xi} e^{-u/\xi}\, du = \xi^q \int_{x=0}^{\infty} x^q e^{-x}\, dx = q!\,\xi^q. \tag{14}$$

Assuming scaling holds exactly across all orders, the above is precisely $\langle (l_1^{(s)})^q\rangle$. Note that $\langle (l_1^{(s)})^q\rangle = q!\langle l_1^{(s)}\rangle^q$. Since the characteristic length of order ω streams is $(R_{l^{(s)}})^{\omega-1}$, we therefore have

$$\langle (l_\omega^{(s)})^q\rangle = q!\,\xi^q (R_{l^{(s)}})^{(\omega-1)q} = q!\langle l_\omega^{(s)}\rangle^q. \tag{15}$$

Since main stream lengths are sums of stream segment lengths, so are their respective moments. Hence,

$$\begin{aligned}\langle (l_\omega)^q\rangle &= \sum_{k=1}^{\omega} \langle (l^{(s)}{}_k)^q\rangle, \\ &= \sum_{k=1}^{\omega} q!\,\xi^q (R_{l^{(s)}})^{(k-1)q}, \\ &= q!\,\xi^q \sum_{k=1}^{\omega} (R_{l^{(s)}})^{(k-1)q}, \\ &= q!\,\xi^q \frac{(R_{l^{(s)}})^{q\omega}-1}{R_{l^{(s)}}-1}.\end{aligned} \tag{16}$$

We can now determine the log-space separation of moments of main stream length. Using Stirling's approximation [44] that $\ln n! \sim (n+1/2)\ln n - n$ we have

$$\ln\langle (l_\omega)^q\rangle \sim q[\xi + (R_{l^{(s)}})^\omega + \ln q] + C, \tag{17}$$

where C is a constant. The $\ln q$ term inside the square brackets in Eq. (17) creates small deviations from linearity for $1 \leqslant \omega \leqslant 15$. Thus, in agreement with Fig. 9, we expect approximately linear growth of moments in log space.

VII. LIMITATIONS ON THE PREDICTIVE POWER OF HORTON'S LAWS

In this last section, we briefly examine deviations from scaling within this generalized picture of Horton's laws. The basic question is, given an approximate scaling for quantities measured at intermediate stream orders, what can we say about the features of the overall basin?

As noted in the previous section, all moments of the generalized Horton distributions grow exponentially with order. Coupling this with the fact that $n_\omega \propto R_n^{-\omega}$, i.e., the number of samples of order ω basins decreases exponentially with ω, we observe that a basin's a and l will potentially differ greatly from values predicted by Horton's laws.

To illustrate this, Fig. 10 specifically shows the distributions $P(l_3)$ and $P(l_4)$ scaled up to give $P(l_{11})$ for the Congo river. The Congo's actual length measured at this 1000-m resolution is represented by the solid line and is around 57% of the distribution's mean, as indicated by the dashed line. Nevertheless, we see that the measured length is within a standard deviation of the predicted value.

In Table IV, we provide a comparison of predicted versus measured main stream lengths and areas for the basins studied here. The mean for the scaled up distributions overestimates the actual values in all cases except for the Nile. Also, apart from the Nile, all values are within a standard deviation of the predicted mean. The coefficients of varia-tion, $\sigma_a/\overline{a}_\Omega$

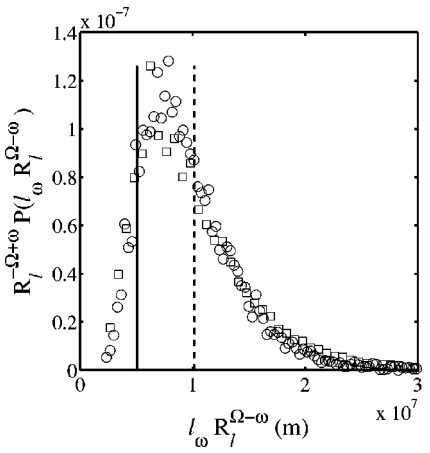

FIG. 10. Comparing the generalized Horton length distribution rescaled to the level of order $\Omega=11$ basins with the Congo River itself. Lengths are in kilometers. The two distributions are for orders $\omega=3$ (squares) and $\omega=4$ (circles) stream lengths and the Horton ratio is estimated to be $R_l=2.39$. The dashed line represents the mean of these scaled up distributions, while the solid line marks $\overline{l}_{11}$, the measured length of the Congo at a 1000-m resolution. The actual length is within a standard deviation of the mean being around 50% of $\overline{l}_{11}$. Table IV shows comparisons for various river networks for both area and length data.

and $\sigma_l/\overline{l}_\Omega$, all indicate that fluctuations are on the order of the expected values of stream lengths and areas.

Thus, we see that by using a probabilistic point of view, this generalized notion of Horton's laws provides a way of discerning the strength of deviations about the expected mean. In general, stronger deviations would imply that geologic conditions play a more significant role in setting the structure of the network.

VIII. CONCLUSION

The objective of this work has been to explore the underlying distributions of river network quantities defined with stream ordering. We have shown that functional relationships generalize all cases of Horton's laws. We have identified the basic forms of the distributions for stream segment lengths (exponential) and main stream lengths (convolutions of exponentials) and shown a link between number and area distributions. Data from the continent-scale networks of the Mississippi, Amazon, and Nile river basins as well as from Scheidegger's model of directed random networks provides both agreement with and inspiration for the generalizations of Horton's laws. Finally, we have identified a fluctuation length scale ξ that is a reinterpretation of what was previously identified as only a mean value. We see the study of the generalized Horton distributions as integral to increasing our understanding of river network structure. We also suggest that practical network analysis be extended to measurements of distributions and the length scale ξ with the aim of refining our ability to distinguish and compare network structure.

By taking account of fluctuations inherent in network scaling laws, we are able to see how measuring Horton's laws on low-order networks is unavoidably problematic. Moreover, as we have observed, the measurement of the Horton ratios is in general a delicate operation, suggesting that many previous measurements are not without error.

The theoretical understanding of the growth and evolution of river networks requires a more thorough approach to measurement and a concurrent improvement in the statistical description of river network geometry. The present consideration of a generalization of Horton's laws is a necessary step in this process, giving rise to stronger tests of both real and synthetic data. In the following paper [21], we round out this expanded picture of network structure by considering the spatial distribution of network components.

ACKNOWLEDGMENTS

The work was supported in part by NSF Grant No. EAR-9706220 and the U.S. Department of Energy, Grant No. DE FG02-99ER 15004. The authors would like to express their gratitude to H. Cheng for enlightening and enabling discussions.

APPENDIX: ANALYTIC CONNECTIONS BETWEEN STREAM LENGTH DISTRIBUTIONS

In this appendix, we consider a series of analytic calculations. These concern the connections between the distributions of stream segment lengths $l_\omega^{(s)}$, ordered basin main stream lengths l_ω, and main stream lengths l. We will idealize the problem in places, assuming perfect scaling and infinite networks, while making an occasional salubrious approximation. Also, we will treat the problem of lengths fully noting that derivations of distributions for areas follow similar, but more complicated lines.

TABLE IV. Comparison of predicted versus measured main stream lengths for large scale river networks. The dimensions of all lengths and areas are 10^6 m and 10^{12} m^2, respectively. Here, l_Ω is the actual main stream length of the basin, $\overline{l}_\Omega$ the predicted mean value of l_Ω, σ_l the predicted variance, and $\sigma_l/\overline{l}_\Omega$ the normalized deviation. The entries for the basin area data have corresponding definitions.

Basin	l_Ω	$\overline{l}_\Omega$	σ_l	$l_\Omega/\overline{l}_\Omega$	$\sigma_l/\overline{l}_\Omega$	a_Ω	$\overline{a}_\Omega$	σ_a	$a_\Omega/\overline{a}_\Omega$	$\sigma_a/\overline{a}_\Omega$
Mississippi	4.92	11.10	5.60	0.44	0.51	2.74	7.55	5.58	0.36	0.74
Amazon	5.75	9.18	6.85	0.63	0.75	5.40	9.07	8.04	0.60	0.89
Nile	6.49	2.66	2.20	2.44	0.83	3.08	0.96	0.79	3.19	0.82
Congo	5.07	10.13	5.75	0.50	0.57	3.70	10.09	8.28	0.37	0.82
Kansas	1.07	2.37	1.74	0.45	0.73	0.14	0.49	0.42	0.28	0.86

We begin by rescaling the form of stream segment length distributions

$$P(l_\omega^{(s)},\omega)=(R_n-1)(R_nR_{l^{(s)}})^{-\omega}F_{l^{(s)}}(lR_{l^{(s)}}^{-\omega}). \quad \text{(A1)}$$

The normalization $C_{l^{(s)}}=R_n-1$ stems from the requirement that

$$\int_{u=0}^{\infty}F_{l^{(s)}}(u)=1, \quad \text{(A2)}$$

which is made purely for aesthetic purposes. As we have suggested in Eq. (8) and demonstrated empirical support for, $F_{l^{(s)}}(u)$ is well approximated by the exponential distribution $\xi^{-1}e^{-u/\xi}$. For low u and also we have noted that deviations do of course occur, but they are sufficiently insubstantial as to be negligible for a first-order treatment of the problem.

1. Distributions of main stream lengths as a function of stream order

We now derive a form for the distribution of main stream lengths $P(l_\omega|\omega)$. As we have discussed, since $l_\omega=\sum_{i=1}^{\omega}l_\omega^{(s)}$, we have the convolution (9). The right-hand side of Eq. (9) consists of exponentials as per Eq. (8), so we now consider the function $K_\omega(u;\vec{a})$ given by

$$K_\omega(u;\vec{a})=a_1e^{-a_1u}*a_2\epsilon^{-a_2u}*\cdots*a_\omega e^{-a_\omega u}, \quad \text{(A3)}$$

where $\vec{a}=(a_1,a_2,\ldots,a_\omega)$. We are specifically interested in the case when no two of the a_i are equal, i.e., $a_i\neq a_j$ for all $i\neq j$. To compute this ω-fold convolution, we simply examine the $K_\omega(u;\vec{a})$ for $\omega=2$ and $\omega=3$ and identify the emerging pattern. For $\vec{a}=(a_1,a_2)$ we have, omitting the prefactors for the time being,

$$e^{-a_1u}*e^{-a_2u}=\frac{e^{-a_1u}-e^{-a_2u}}{a_1-a_2}=\frac{e^{-a_1u}}{a_1-a_2}+\frac{e^{-a_2u}}{a_2-a_1} \quad \text{(A4)}$$

providing $a_1\neq a_2$. Convolving this with e^{-a_3u}, we obtain

$$\begin{aligned}e^{-a_1u}*e^{-a_2u}*e^{-a_3u}&=\left(\frac{e^{-a_1u}-e^{-a_2u}}{a_1-a_2}\right)*e^{-a_3u}\\&=\frac{e^{-a_1u}-e^{-a_3u}}{(a_1-a_2)(a_1-a_3)}-\frac{e^{-a_2u}-e^{-a_3u}}{(a_1-a_2)(a_2-a_3)}\\&=\frac{e^{-a_1u}}{(a_1-a_2)(a_1-a_3)}+\frac{e^{-a_2u}}{(a_2-a_1)(a_2-a_3)}\\&\quad+\frac{e^{-a_3u}}{(a_3-a_1)(a_3-a_2)}. \quad \text{(A5)}\end{aligned}$$

Generalizing from this point, we have

$$K_\omega(u;\vec{a})=\left(\prod_{i=1}^{\omega}a_i\right)\sum_{i=1}^{\omega}\frac{e^{-a_iu}}{\prod_{j=1,j\neq i}^{\omega}(a_i-a_j)}. \quad \text{(A6)}$$

Now, setting $a_i=1/(\xi(R_{l^{(s)}})^{i-1})$ and carrying out some manipulations we obtain the following expression for $P(l_\omega,\omega)$:

$$\begin{aligned}P(l_\omega,\omega)&=\frac{1}{(R_n)^\omega}\frac{1}{\prod_{j=1}^{\omega}\xi(R_{l^{(s)}})^{i-1}}\sum_{i=1}^{\omega}\frac{e^{-l_\omega/\xi(R_{l^{(s)}})^{i-1}}}{\prod_{j=1,j\neq i}^{\omega}[1/\xi(R_{l^{(s)}})^{i-1}-1/\xi(R_{l^{(s)}})^{j-1}]}\\&=\frac{1}{(R_n)^\omega}\frac{1}{\prod_{j=1}^{\omega}(R_{l^{(s)}})^{j-1}}\sum_{i=1}^{\omega}e^{-l_\omega/\xi(R_{l^{(s)}})^{i-1}}\xi^{\omega-1}\frac{\prod_{j=1,j\neq i}^{\omega}(R_{l^{(s)}})^{i-1}\prod_{j=1,j\neq i}^{\omega}(R_{l^{(s)}})^{j-1}}{\prod_{j=1,j\neq i}^{\omega}(R_{l^{(s)}})^{j-1}-(R_{l^{(s)}})^{i-1}}\\&=\frac{1}{(R_n)^\omega}\frac{\xi^{\omega-1}}{\xi^\omega}\sum_{i=1}^{\omega}e^{-l_\omega/\xi(R_{l^{(s)}})^{i-1}}\frac{(R_{l^{(s)}})^{-2(i-1)}\prod_{j=1}^{\omega}(R_{l^{(s)}})^{i-1}\prod_{j=1}^{\omega}(R_{l^{(s)}})^{j-1}\prod_{k=1}^{\omega}(R_{l^{(s)}})^{-(j-1)}}{(R_{l^{(s)}})^{-(\omega-1)}\prod_{j=1,j\neq i}^{\omega}(R_{l^{(s)}})^{j}-(R_{l^{(s)}})^{i}}\\&=\frac{1}{(R_n)^\omega}\frac{1}{\xi}\sum_{i=1}^{\omega}e^{-l_\omega/\xi(R_{l^{(s)}})^{i-1}}\frac{(R_{l^{(s)}})^{(i-1)(\omega-2)}(R_{l^{(s)}})^{\omega-2}/R_{l^{(s)}}}{\prod_{j=1,j\neq i}^{\omega}(R_{l^{(s)}})^{j}-(R_{l^{(s)}})^{i}}\\&=\frac{1}{(R_n)^\omega}\frac{1}{\xi R_{l^{(s)}}}\sum_{i=1}^{\omega}e^{-l_\omega/\xi(R_{l^{(s)}})^{i-1}}\frac{(R_{l^{(s)}})^{i(\omega-2)}}{\prod_{j=1,j\neq i}^{\omega}(R_{l^{(s)}})^{j}-(R_{l^{(s)}})^{i}}. \quad \text{(A7)}\end{aligned}$$

Note that we have added in a factor of $1/(R_n)^{\omega}$ for the appropriate normalization. In addition, one observes that $P(0,\omega)=0$ for all $\omega>1$ since all convolutions of pairs of exponentials vanish at the origin. Furthermore, the tail of the distribution is dominated by the exponential corresponding to the largest stream segment.

The next step is to connect to the power-law distribution of main stream lengths, $P(l)$ (see Fig. 7 and the accompanying discussion). On considering Eq. (10), we see that the problem can possibly be addressed with some form of asymptotic analysis.

Before attacking this calculation, however, we will simplify the notation keeping only the important details of the $P(l_\omega,\omega)$. Our main interest is to see how Eq. (10) gives rise to a power law. We transform the outcome of Eq. (A7) by using $n=\omega$, $u=l_\omega/\xi$, $r=R_{l(s)}$, and $s=R_n$, neglecting multiplicative constants and then summing over stream orders to obtain

$$G(u)=\sum_{n=1}^{\infty}\frac{1}{s^n}\sum_{i=1}^{n}\frac{r^{(n-2)i}e^{-u/r^{i-1}}}{\prod_{j=1,j\neq i}^{n}(r^j-r^i)}. \tag{A8}$$

The integration over l_ω has been omitted, meaning that the result will be a power law with one power lower than expected.

2. Power-law distributions of main stream lengths

We now show that this sum of exponentials $G(u)$ in Eq. (A8) does in fact asymptotically tend to a power law. We first interchange the order of summation replacing $\Sigma_{n=1}^{\infty}\Sigma_{i=1}^{n}$ with $\Sigma_{i=1}^{\infty}\Sigma_{n=i}^{n}$ to give

$$G(u)=\sum_{i=1}^{\infty}e^{-u/r^{i-1}}\sum_{n=1}^{\infty}\frac{r^{(n-2)i}}{s^n\prod_{j=1,j\neq i}^{n}(r^j-r^i)},$$

$$=\sum_{i=1}^{\infty}C_i e^{-u/r^{i-1}}. \tag{A9}$$

We thus simply have a sum of exponentials to contend with. The coefficients C_i appear unwieldy at first, but do yield a simple expression after some algebra that we now perform:

$$C_i=\sum_{n=1}^{\infty}\frac{r^{(n-2)i}}{s^n\prod_{j=1,j\neq i}^{n}(r^j-r^i)} \tag{A10}$$

$$=\frac{1}{\prod_{j=1}^{i-1}(r^j-r^i)}\sum_{n=i}^{\infty}\frac{r^{(n-2)i}}{s^n\prod_{j=i+1}^{n}(r^j-r^i)}$$

$$=\frac{r^{(i-2)i}}{\prod_{j=1}^{i-1}(r^j-r^i)}\frac{1}{s^i}\sum_{n=i}^{\infty}\frac{s^i r^{(n-2)i}r^{-(i-2)i}}{s^n\prod_{j=i+1}^{n}(r^j-r^i)}$$

$$=\frac{1}{\prod_{j=1}^{i-1}r^{-i}(r^j-r^i)}\frac{r^{-i}}{s^i}\sum_{n=i}^{\infty}\frac{r^{(n-i)i}}{s^{n-i}\prod_{j=i+1}^{n}(r^j-r^i)}$$

$$=\frac{1}{\prod_{j=1}^{i-1}(r^{j-i}-1)}\frac{1}{r^i s^i}\sum_{n=i}^{\infty}\frac{1}{\prod_{j=i+1}^{n}sr^{-i}(r^j-r^i)}$$

$$=\frac{1}{r^i s^i}\frac{1}{\prod_{j=1}^{i-1}(r^{j-i}-1)}\sum_{n=i}^{\infty}\prod_{j=i+1}^{n}\frac{1}{s(r^{j-i}-1)}$$

$$=\frac{1}{r^i s^i}\frac{1}{\prod_{j=1}^{i-1}(r^{j-i}-1)}\sum_{n=i}^{\infty}\prod_{j=i+1}^{n}\frac{1}{s(r^{j-i}-1)}$$

$$=\frac{1}{r^i s^i}\left(\frac{-1}{\prod_{k=1}^{i-1}(1-r^{-k})}\right)\left(\sum_{m=1}^{\infty}\prod_{k=1}^{m}\frac{1}{s(r^k-1)}\right).$$

In reaching the last line, we have shifted the indices in several places. In the last bracketed term we have set $k=j-i$ and then $m=n-i$, while in the first bracketed term, we have used $-k=j-i$. Immediately of note is that the last term is independent of i and may thus be ignored.

The first bracketed term does depend on i, but converges rapidly. Writing $D_i=\Pi_{k=1}^{i-1}(1-r^{-k})$ we have that $D_i=D_m\Pi_{k=m}^{i-1}(1-r^{-k})$. Taking m to be fixed and large enough such that $1-r^{-k}$ is approximated well by $\exp\{-r^{-k}\}$ for $k\geqslant m$, we then have

$$D_i=D_m\exp\left\{\sum_{k=m}^{i-1}-r^{-k}\right\}$$

$$=D_m\exp\left\{\frac{r^{1-m}}{(r-1)}(1-1/r^{i-m-1})\right\}. \tag{A11}$$

As $i\to\infty$, D_i clearly approaches a product of D_m and a constant. Therefore, the first bracketed term in Eq. (A10) may also be neglected in an asymptotic analysis.

Hence, as $i\to\infty$, the coefficients C_i are simply given by

$$C_i\propto\frac{1}{s^i r^i}, \tag{A12}$$

and we can approximate $G(u)$ as, boldly using the equality sign,

$$G(u)=AS(u)=A\sum_{i=0}^{\infty}\frac{e^{-u/r^i}}{r^{i(1+\gamma)}}, \tag{A13}$$

where A comprises the constant part of the C_i and factors picked up by shifting the lower limit of the index i from 1 to 0. We have also used here the identification

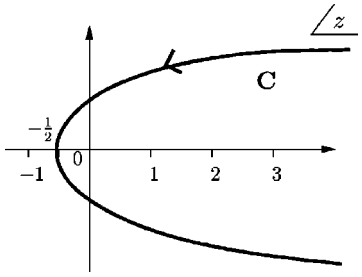

FIG. 11. Contour C used for evaluation of the integral given in Eq. (A16). The poles are situated at $n+0i$ where $n\in\{0,1,2,\ldots\}$.

$$s=r^{\gamma}. \tag{A14}$$

We turn now to the asymptotic behavior of $S(u)$, this being the final stretch of our analysis.

There are several directions one may take at this point. We will proceed by employing a transformation of $S(u)$ that is sometimes referred to as the Sommerfeld-Watson transformation and also as Watson's lemma ([45], p. 239). Given a sum over any set of integers I, say $S=\Sigma_{n\in I}f(n)$, it can be written as the following integral:

$$S=\frac{1}{2\pi i}\oint_C \frac{\pi\cos\pi z}{\sin\pi z}f(z)dz, \tag{A15}$$

where C is a contour that contains the points on the real axis $n+i0$ where $n\in I$ and none of the points of the same form with $n\in\mathbb{Z}/I$. Calculation of the residues of the simple poles of the integrand return us to the original sum.

Applying the transformation to $S(u)$, we obtain

$$S(u)=\frac{1}{2\pi i}\oint_C \frac{\pi\cos\pi z}{\sin\pi z}e^{-ur^{-z}}r^{-z(1+\gamma)}dz. \tag{A16}$$

The contour C is represented in Fig. 11.

We first make a change of variables, $r^{-z}=\rho$. Substituting this and $dz=-d\rho/\rho\ln r$ into Eq. (A16) we have

$$\begin{aligned}S(u)&=\frac{1}{2\pi i}\oint_C{}' \frac{\pi\cos(-\pi\ln\rho/\ln r)}{\sin(-\pi\ln\rho/\ln r)}\\&\quad\times e^{-u\rho}\rho^{(1+\gamma)}(-d\rho/\rho\ln r)\\&=\frac{1}{2i\ln r}\oint_C{}' \frac{\pi\cos(-\pi\ln\rho/\ln r)}{\sin\pi\ln\rho/\ln r}e^{-u\rho}\rho^{\gamma}d\rho.\end{aligned} \tag{A17}$$

The transformed contour C' is depicted in Fig. 12.

As $u\to\infty$, the contribution to integral from the neighborhood of $\rho=0$ dominates. The introduction of the sin and cos terms has created an interesting oscillation that has to be handled with some care. We now deform the integration contour C' into the contour C'' of Fig. 13 focusing on the interval along the imaginary axis $[-i,i]$. Choosing this path will simplify the cos and sin expressions, which at present have logs in their arguments.

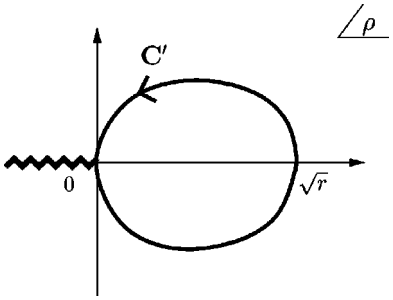

FIG. 12. Contour C' used for evaluation of the integral given in Eq. (A17) as deduced from contour C (Fig. 11) with the transformation $\rho=r^{-z}$. The negative real axis is a branch cut.

The integral $S(u)$ is now given by $S(u)\simeq I(u)+\text{c.c.}$, where

$$I(u)=\frac{-1}{2i\ln r}\int_0^i \frac{\pi\cos\pi\ln\rho/\ln r}{\sin\pi\ln\rho/\ln r}e^{-u\rho}\rho^{\gamma}d\rho. \tag{A18}$$

Writing $\rho=\sigma+i\tau$ with $\sigma=0$, we have $d\rho=id\tau$ and the following for the cos and sin terms:

$$\begin{aligned}\cos\pi\ln\rho/\ln r&=\frac{\rho^{i\pi/\ln r}+\rho^{-i\pi/\ln r}}{2}\\&=\frac{\tau^{i\pi/\ln r}e^{-\pi^2/2\ln r}+\tau^{-i\pi/\ln r}e^{\pi^2/2\ln r}}{2},\end{aligned} \tag{A19}$$

and

$$\begin{aligned}\sin\pi\ln\rho/\ln r&=\frac{\rho^{i\pi/\ln r}-\rho^{-i\pi/\ln r}}{2i}\\&=\frac{\tau^{i\pi/\ln r}e^{-\pi^2/2\ln r}-\tau^{-i\pi/\ln r}e^{\pi^2/2\ln r}}{2i}.\end{aligned} \tag{A20}$$

The cot term in the integrand becomes

$$\frac{\cos\pi\ln\rho/\ln r}{\sin\pi\ln\rho/\ln r}=-i\frac{1+\tau^{2i\pi/\ln r}e^{-\pi^2/\ln r}}{1-\tau^{2i\pi/\ln r}e^{-\pi^2/\ln r}}=-i\frac{1+\delta(\tau)}{1-\delta(\tau)}, \tag{A21}$$

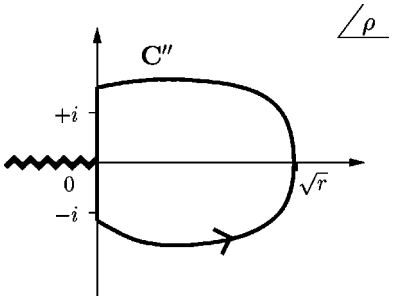

FIG. 13. Contour C'' used for evaluation of the integral given in Eq. (A16). The poles are situated at $n+0i$ where $n\in\{0,1,2,\ldots\}$.

where $\delta(\tau)=\tau^{2i\pi/\ln r}e^{-\pi^{2/\ln r}}$. The integral $I(u)$ now becomes

$$I(u)=\frac{i}{2\ln r}\int_0^1\frac{1+\delta(\tau)}{1-\delta(\tau)}e^{-iu\tau}\tau^{\gamma}e^{i\pi\gamma/2}\,d\tau$$

$$=\frac{e^{i\pi(1+\gamma)/2}}{2\ln r}\int_0^1 e^{-iur}\tau^{\gamma}\frac{1+\delta(\tau)}{1-\delta(\tau)}\,d\tau. \qquad \text{(A22)}$$

Now, since $|\delta(\tau)|=e^{-\pi^{2/\ln r}}\lesssim 10^{-4}$ (taking $r=R_{l(s)}\approx 2.5$), we can expand the expression as follows:

$$\frac{1+\delta}{1-\delta}=(1+\delta)(1+\delta+\delta^2+\cdots)$$

$$=1+2\delta+2\delta^2+2\delta^3+\cdots. \qquad \text{(A23)}$$

The integral in turn becomes

$$I(u)=\frac{i^{1+\gamma}}{2\ln r}\int_0^1 d\tau\,\tau^{\gamma}e^{-iu\tau}(1+2\tau^{2i\pi/\ln r}e^{-\pi^2/\ln r}$$

$$+2\tau^{4i\pi/\ln r}e^{-2\pi^2/\ln r}+\cdots+2\tau^{2ni\pi/\ln r}e^{-n\pi^2/\ln r}+\cdots). \qquad \text{(A24)}$$

The basic nth integral in this expansion is

$$I_n(u)=\int_0^1\tau^{\gamma+2ni\pi/\ln r}e^{-iu\tau}\,d\tau. \qquad \text{(A25)}$$

Substituting $u\tau=w$ and replacing the upper limit $w=u$ with $w=\infty$ we have

$$I_n(u)=u^{-(1+\gamma+2ni\pi/\ln r)}\int_0^{\infty}dw\,w^{\gamma+2ni\pi/\ln r}e^{-iw}$$

$$=(iu)^{-(1+\gamma+2ni\pi/\ln r)}\int_0^{\infty}i\,dw(iw)^{\gamma+2ni\pi/\ln r}e^{-iw}$$

$$=(iu)^{-(1+\gamma+2ni\pi/\ln r)}\int_0^{\infty}dv(v)^{\gamma+2ni\pi/\ln r}e^{-v}$$

$$=(iu)^{-(1+\gamma+2ni\pi/\ln r)}\Gamma(\gamma+2ni\pi/\ln r). \qquad \text{(A26)}$$

Here, we have rotated the contour along the imaginary iw axis to the real v axis and identified the integral with the gamma function Γ [44]. The integral can now be expressed as

$$I(u)=\frac{1}{2\ln r u^{1+\gamma}}\left[1+2\sum_{n=1}^{\infty}u^{-2ni\pi/\ln r}\Gamma(\gamma+2ni\pi/\ln r)\right]. \qquad \text{(A27)}$$

We now need to show that the higher-order terms are negligible. Note that their magnitudes do not vanish with increasing u, but instead are highly oscillatory terms. Using the asymptotic form of the Gamma function [46]

$$\Gamma(z)=z^{z-1/2}e^{-z}\sqrt{2\pi}[1+O(1/z)], \qquad \text{(A28)}$$

we can estimate as follows for large n that

$$|\Gamma(1+\gamma+2ni\pi/\ln r)|$$

$$\sim|(2i\pi n/\ln r+1+\gamma)^{2i\pi n/\ln r+1/2+\gamma}e^{-\gamma-1}\sqrt{2\pi}|$$

$$=|(e^{i\pi/2}2\pi n/\ln r)^{2i\pi n/\ln r+1/2+\gamma}e^{-\gamma-1}\sqrt{2\pi}|$$

$$=e^{-\pi^2 n/\ln r}n^{\gamma+1/2}(2\pi/e)^{1+\gamma}(\ln r)^{-1/2-\gamma}. \qquad \text{(A29)}$$

Hence, $\Gamma(1+\gamma+2ni\pi/\ln r)$ vanishes exponentially with n. For the first few values of n taking $\gamma=3/2$ and $r=2.5$, we have $\Gamma(1+\gamma+2i\pi/\ln r)\simeq 2.5\times 10^{-3}$ and $\Gamma(1+\gamma+4i\pi/\ln r)\simeq 2.1\times 10^{-6}$ showing that these corrections are negligible.

Hence we are able to estimate $S(u)$ to first order as

$$S(u)\simeq\frac{1}{\ln r}u^{-1-\gamma}. \qquad \text{(A30)}$$

Thus, we have determined that a power law follows from the initial assumption that stream segment lengths follow exponential distributions.

This equivalence has been drawn as an asymptotic one, albeit one where convergences have been shown to be rapid. The calculation is clearly not the entire picture as the solution does contain small rapidly-oscillating corrections that do not vanish with increasing argument. A possible remaining problem and one for further investigation is to understand how the distributions for main stream lengths l_ω fit together over a range that is not to be considered asymptotic. Nevertheless, the preceding is one attempt at demonstrating this rather intriguing breakup of a smooth power law into a discrete family of functions built up from one fundamental scaling function.

[1] I. Rodríguez-Iturbe and A. Rinaldo, *Fractal River Basins: Chance and Self-Organization* (Cambridge University Press, Cambridge, UK, 1997).

[2] A. Rinaldo, I. Rodríguez-Iturbe, and R. Rigon, Annu. Rev. Earth Planet Sci. **26**, 289 (1998).

[3] P. S. Dodds and D. H. Rothman, Annu. Rev. Earth Planet Sci. **28**, 571 (2000).

[4] W. B. Langbein, U.S. Geol. Surv. Water-Supply Pap. W **0968-C**, 125 (1947).

[5] J. T. Hack, U.S. Geol. Surv. Prof. Pap. **294-B**, 45 (1957).

[6] A. D. Abrahams, Water Resour. Res. **20**, 161 (1984).

[7] A. Maritan, A. Rinaldo, R. Rigon, A. Giacometti, and I. Rodríguez-Iturbe, Phys. Rev. E **53**, 1510 (1996).

[8] P. S. Dodds and D. H. Rothman, Phys. Rev. E **59**, 4865 (1999).

[9] T. Sun, P. Meakin, and T. Jøssang, Phys. Rev. E **49**, 4865 (1994).

[10] A. Rinaldo, I. Rodríguez-Iturbe, R. Rigon, E. Ijjasz-Vasquez,

and R. L. Bras, Phys. Rev. Lett. **70**, 822 (1993).
[11] C. P. Stark, Nature (London) **352**, 405 (1991).
[12] L. B. Leopold and W. B. Langbein, U.S. Geol. Surv. Prof. Pap. **500-A**, 1 (1962).
[13] A. E. Scheidegger, Bull. Int. Assoc. Sci. Hydrol. **12**, 15 (1967).
[14] S. S. Manna, D. Dhar, and S. N. Majumdar, Phys. Rev. A **46**, 4471 (1992).
[15] A. Maritan, F. Colaiori, A. Flammini, M. Cieplak, and J. R. Banavar, Science **272**, 984 (1996).
[16] P. S. Dodds and D. H. Rothman, preceding paper, Phys. Rev. E **63**, 016115 (2001).
[17] R. E. Horton, Bull. Geol. Soc. Am. **56**, 275 (1945).
[18] S. A. Schumm, Bull. Geol. Soc. Am. **67**, 597 (1956).
[19] B. B. Mandelbrot, *The Fractal Geometry of Nature* (Freeman, San Francisco, 1983).
[20] S. Peckham and V. Gupta, Water Resour. Res. **35**, 2763 (1999).
[21] P. S. Dodds and D. H. Rothman, following paper, Phys. Rev. E **63**, 016117 (2001).
[22] A. N. Strahler, EOS Trans. Am. Geophys. Union **38**, 913 (1957).
[23] M. Zamir, S. M. Wrigley, and B. L. Langille, J. Gen. Physiol. **81**, 325 (1983).
[24] Y.-C. B. Fung, *Biomechanics: Motion, Flow, Stress, and Growth* (Springer-Verlag, New York, 1990).
[25] G. S. Kassab, C. A. Rider, T. N. J., and Y. B. Fung, Am. J. Physiol. **265**, H350 (1993).
[26] G. S. Kassab and Y.-C. B. Fung, Am. J. Physiol. **267**, H319 (1994).
[27] G. S. Kassab, D. H. Lin, and Y.-C. B. Fung, Am. J. Physiol. **267**, H2100 (1994).
[28] D. L. Turcotte, J. D. Pelletier, and W. I. Newman, J. Theor. Biol. **193**, 577 (1998).
[29] S. Aharinejad, W. Schreiner, and F. Neumann, Anat. Rec. **251**, 50 (1998).
[30] M. Zamir, J. Theor. Biol. **197**, 517 (1999).
[31] J. W. Kirchner, Geology **21**, 591 (1993).
[32] D. G. Tarboton, R. L. Bras, and I. Rodríguez-Iturbe, Water Resour. Res. **24**, 1317 (1988).
[33] P. La Barbera and R. Rosso, Water Resour. Res. **25** (4), 735 (1989).
[34] D. G. Tarboton, R. L. Bras, and I. Rodríguez-Iturbe, Water Resour. Res. **26**, 2243 (1990).
[35] H. de Vries, T. Becker, and B. Eckhardt, Water Resour. Res. **30**, 3541 (1994).
[36] The Mississippi river network was extracted from a topography dataset composed of digital elevations models obtained from the U.S. Geological Survey and are available on the Internet at www.usgs.gov. The dataset is decimated so as to have horizontal resolution of approximately 1000 m leading to an order $\Omega = 11$ network.
[37] The topography dataset used for the Amazon was obtained from the website of the National Imagery and Mapping Agency (www.nima.mil). The dataset has a horizontal resolution of approximately 1000 m yielding and order $\Omega = 11$ network for the Amazon.
[38] The data for the Nile come from the U.S. Geological Survey's 30 arc second HydrolK dataset, available on the Internet at edcftp.cr.usgs.gov, which has a grid spacing of approximately 1000 m. At this resolution, the Nile is an order $\Omega = 10$ basin.
[39] W. Feller, *An Introduction to Probability Theory and Its Applications* (John Wiley & Sons, New York, 1968), Vol. I.
[40] E. Tokunaga, Geophys. Bull. Hokkaido Univ. **15**, 1 (1966).
[41] E. Tokunaga, Geogr. Rep., Tokyo Metrop. Univ. **13**, 1 (1978).
[42] E. Tokunaga, Trans. Jpn. Geomorphol. Union **5**, 71 (1984).
[43] S. D. Peckham, Water Resour. Res. **31**, 1023 (1995).
[44] I. Gradshteyn and I. Ryzhik, *Table of Integrals, Series, and Products*, 5th ed. (Academic Press, San Diego, 1994).
[45] G. F. Carrier, M. Krook, and C. E. Pearson, *Functions of a Complex Variable; Theory and Technique* (McGraw-Hill, New York, 1966).
[46] C. M. Bender and S. A. Orszag, *Advanced Mathematical Methods for Scientists and Engineers*, International Series in Pure and Applied Mathematics (McGraw-Hill, New York, 1978).